Mesoscale networks and corresponding transitions from self-assembly of block copolymers

Cheng-Yen Chang[a,1], Gkreti-Maria Manesi[b,1], Chih-Ying Yang[c], Yu-Chueh Hung[c], Kai-Chieh Yang[a], Po-Ting Chiu[a], Apostolos Avgeropoulos[b,2], and Rong-Ming Ho[a,2]

[a]Department of Chemical Engineering, National Tsing Hua University, Hsinchu 30013, Taiwan, Republic of China; [b]Department of Materials Science Engineering, University of Ioannina, Ioannina 45110, Greece; and [c]Institute of Photonics Technologies, National Tsing Hua University, Hsinchu 30013, Taiwan, Republic of China

Edited by David A. Weitz, Harvard University, Cambridge, MA, and approved February 1, 2021 (received for review October 25, 2020)

A series of cubic network phases was obtained from the self-assembly of a single-composition lamellae (L)-forming block copolymer (BCP) polystyrene-block-polydimethylsiloxane (PS-*b*-PDMS) through solution casting using a PS-selective solvent. An unusual network phase in diblock copolymers, double-primitive phase (DP) with space group of $Im\bar{3}m$, can be observed. With the reduction of solvent evaporation rate for solution casting, a double-diamond phase (DD) with space group of $Pn\bar{3}m$ can be formed. By taking advantage of thermal annealing, order–order transitions from the DP and DD phases to a double-gyroid phase (DG) with space group of $Ia\bar{3}d$ can be identified. The order–order transitions from DP (hexapod network) to DD (tetrapod network), and finally to DG (trigonal planar network) are attributed to the reduction of the degree of packing frustration within the junction (node), different from the predicted Bonnet transformation from DD to DG, and finally to DP based on enthalpic consideration only. This discovery suggests a new methodology to acquire various network phases from a simple diblock system by kinetically controlling self-assembling process.

double-primitive network | double diamond | double gyroid | self-assembly | order–order transitions

From constituted molecules to polymers, finally ordered hierarchical superstructures, self-assembled solids cover a vast area of nanostructures where the characters of building blocks direct the progress of self-assembly (1, 2). In nature, fascinating periodic network structures and morphologies from different species are appealing in nanoscience and nanotechnology due to their superior properties, especially for photonic crystal structures (3–7). For gyroid, trigonal planar network with chirality demonstrates its potential as chiropitc metamaterial (8–10). Beyond the splendid colors, networks either in macroscale or mesoscale mechanically strengthen their skeletons and protect those fragile but vital organs from impact (11, 12). Inspired by nature, biomimicking materials with mesoscale network may exceed the limitation of the intrinsic properties (13). The topology of networks could further improve their adaptability, allowing extreme deformation for energy dissipation (14). Moreover, network materials from hybridization of self-assembled block copolymers (BCPs) have been exploited to the design of mesoscale quantum metamaterials (15, 16). With the desire to acquire network textures for biomimicking nanomaterials, BCPs with immiscible constituted segments covalently joined together give the accessibility to the formation of nanonetwork morphologies via balancing enthalpic penalty from the repulsive interaction of constituted blocks and entropic penalty from the stretching of polymer chains (17–21). By taking advantage of precise synthesis procedures, it is feasible to obtain the aimed network phases from the self-assembly of BCPs such as *Fddd* (O^{70}) (22–24), gyroid (Q^{214}, Q^{230}) (20, 21, 25–27), and diamond (Q^{224}, Q^{227}) (28–31) experimentally and theoretically. On the basis of theoretical prediction, the junction points (nodes) in the network phases could be coordinated with three, four, or six neighbors in three-dimensional space, resulting in the enhancement of packing frustration (31). Topologically, all these phases match the coordination number to neighbors ($n = 3, 4, 6$), showing no special case of quasicrystal. Accordingly, an order–order transition from double-diamond phase (DD, tetrapod) to double-gyroid phase (DG, trigonal planar network) has been observed (29). Yet, there is no DP phase being found in simple diblock systems except for liquid crystals (32, 33) or organic–inorganic nanocomposites from the mixtures of BCP with inorganic precursors (34, 35). Searching the rare occurrence of network phases and the corresponding phase transitions among phases will be essential to the demands for application by considering the deliberate structuring effects on aimed properties but the approaches remain challenging (8, 36–40). For instance, viewing the narrow window for network morphologies in diblock copolymer phase diagram, it demands harsh requirements for syntheses (2, 41). Recently, by taking advantage of using selective solvent for solution casting, it is feasible to acquire DG phase and even inverted DG phase from the self-assembly of lamellae (L)-forming polystyrene-block-polydimethylsiloxane (PS-*b*-PDMS) (42). Apart from that, a triclinic DG phase was recently discovered from the PS-*b*-PDMS which is commonly believed nonexisting in the

Significance

Mesoscale networks from the self-assembly of block copolymers (BCPs) demonstrate appealing potentials in a variety of applications such as optical, mechanical, and quantum metamaterials. Herein, three intriguing network phases (double gyroid, double diamond, and double primitive) could be obtained via controlled self-assembly of a simple lamellae-forming polystyrene-block-polydimethylsiloxane diblock copolymer. Kinetically controlled solution-casting and thermal annealing procedures are able to acquire these three metastable phases; in line with the self-consistent field theory, phase transitions start from primitive to diamond, and then to gyroid. Further examinations through small-angle X-ray scattering and electron tomography reveal the phase transitions with epitaxial relationships of the networks and adjustments on curvatures at the high interaction parameter (χ) BCP interface.

Author contributions: A.A. and R.-M.H. designed research; C.-Y.C., G.-M.M., C.-Y.Y., Y.-C.H., K.-C.Y., and P.-T.C. performed research; C.-Y.C. analyzed data; and C.-Y.C. and G.-M.M. wrote the paper.

The authors declare no competing interest.

This article is a PNAS Direct Submission.

Published under the PNAS license.

[1]C.-Y. C. and G.-M. M. contributed equally to this work.

[2]To whom correspondence may be addressed. Email: aavger@uoi.gr, or rmho@mx.nthu.edu.tw.

This article contains supporting information online at https://www.pnas.org/lookup/suppl/doi:10.1073/pnas.2022275118/-/DCSupplemental.

Published March 9, 2021.

Downloaded by guest on February 15, 2022

conventional phase diagram (43). As a result, the phase diagram of BCPs with high interaction parameter is worthy of study for searching the metastable phases with unique network textures (44). Herein, we aim to acquire network phases from a simple diblock system by kinetically controlling the transformation mechanisms of self-assembly. As exemplified by using the PS-*b*-PDMS for solution casting, with the use of a PS-selective solvent (chloroform), a DP phase and a DD phase could be formed through controlled self-assembly, giving unique network phases simply from solution casting. Moreover, a DG phase can be also acquired from phase transformation. Consequently, a series of network phases with hexapod, tetrapod, and trigonal planar building units could be successfully obtained by using a single-composition L-forming PS-*b*-PDMS for self-assembly. The corresponding order–order transitions among these network phases examined by temperature-resolved in situ small-angle X-ray scattering (SAXS) combining with electron tomography results provide insights of network phase formation and the corresponding phase transformation mechanisms in the self-assembly of BCPs.

Results

Characterization of Lamellae-forming PS-*b*-PDMS. A single-composition L-forming PS-*b*-PDMS with the volume fraction of PDMS (f_{PDMS}^{v}) = 0.42 (M_n^{PS}= 51,000 g/mole, M_n^{PDMS}= 35,000 g/mole, $Đ_M$ = 1.05) (see *SI Appendix* for detailed synthetic routes and corresponding characterization) was synthesized and examined after solution casting using a neutral solvent (cyclohexane). The casting was carried out using 10 wt % concentration for solution casting under slow evaporation (0.1 mL/d). As shown in *SI Appendix*, Fig. S3, the stable phase of self-assembled PS-*b*-PDMS observed by transmission electron microscopy (TEM) appears as a typical lamellar projection; with further evidenced by SAXS, the reflections at the relative q values of 1: 2: 3: 4: 5: 6: 8: 9: 10 can be clearly identified, suggesting the formation of a lamellae phase.

Discovery of DP Structure. With the use of a PS-selective solvent, chloroform, for solution casting under slow evaporation (0.1 mL/d), as shown in Fig. 1*A*, SAXS results with the first-order reflections at the relative q values of $\sqrt{2}$:$\sqrt{3}$:$\sqrt{6}$ can be found. We speculate that these reflections are attributed to a DD phase, corresponding to the (110), (111), and (211) reflections (see *SI Appendix*, Fig. S4 for details); the red dashed line in the SAXS profiles indicate the predicted reflections with the relative q values of $\sqrt{2}$:$\sqrt{3}$:$\sqrt{4}$:$\sqrt{6}$:$\sqrt{10}$:$\sqrt{12}$:$\sqrt{14}$:$\sqrt{18}$:$\sqrt{21}$ for characteristic reflections of a DD phase. The suggested DD phase was further identified by TEM along different directions for projections, as shown in Fig. 1 *B*–*E* with [100], [111], [311], and [321] projections. Three-dimensional reconstruction images were acquired by electron tomography in which the tetrapod building unit for the DD phase can be clearly identified (*SI Appendix*, Fig. S6). Interestingly, with the acceleration of evaporation rate (0.1 mL/h, referred as fast evaporation) for solution casting, two additional reflection can be found in the low-q region as shown in Fig. 1*A*; we speculate that it might be attributed to the distortion of the diamond networks. Subsequently, real-space imaging

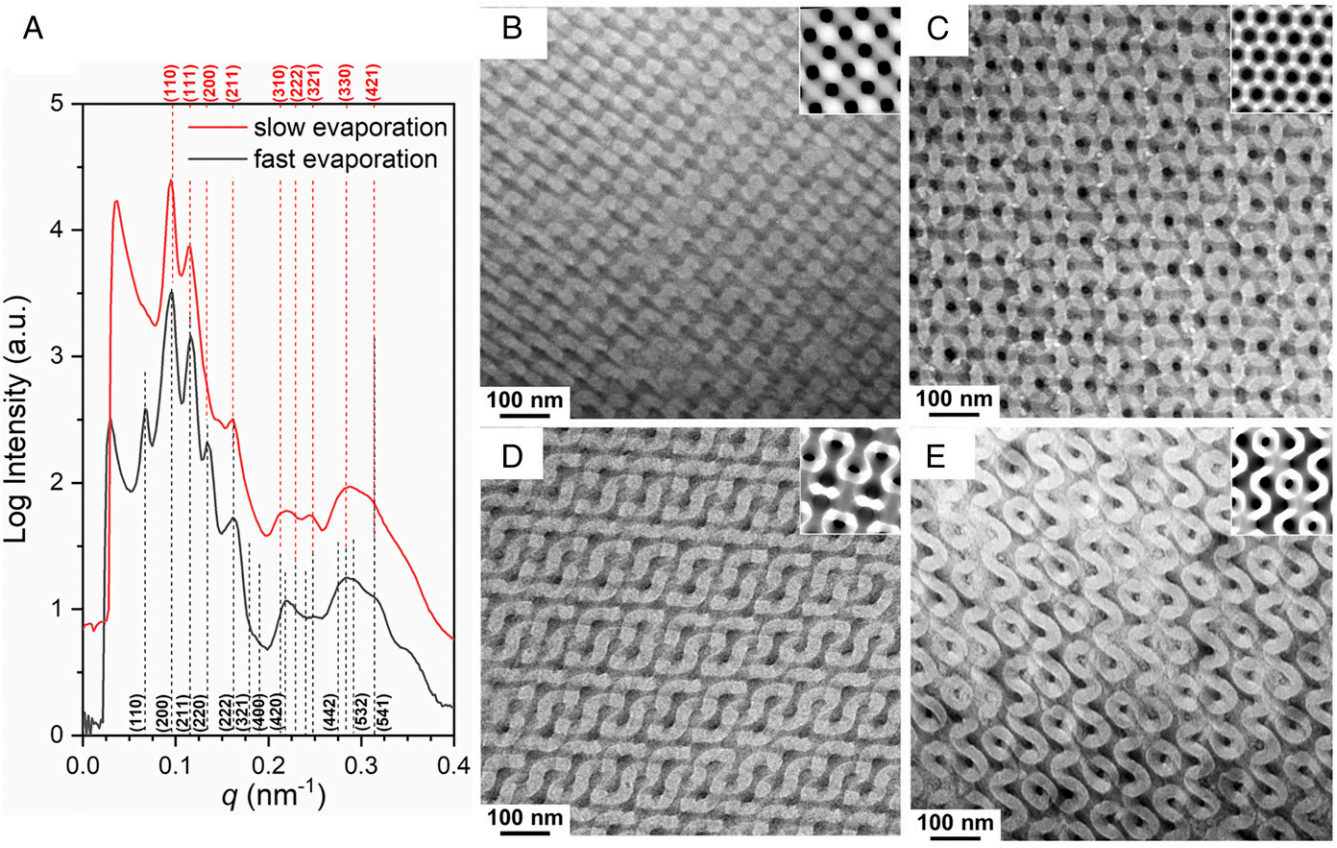

Fig. 1. (*A*) One-dimensional (1D) SAXS profiles of PS-*b*-PDMS after casting from slow and fast evaporation rates. The red dashed lines are the reflection planes referred to $Pn\bar{3}m$ (DD) at which two additional peaks could be clearly identified in the low-q region. The black dashed lines are the reflection planes based on DP phase with space group $Im\bar{3}m$, giving the reflections of (110) and (220). TEM micrographs of fast-evaporated PS-*b*-PDMS along various projection directions: (*B*) [100]; (*C*) [111]; (*D*) [311]; and (*E*) [321] for DD phase. (*Insets*) The corresponding images from simulation based on DD phase.

Downloaded by guest on February 15, 2022

under TEM was carried out; as found, there are unexpected projections (Fig. 2 *A*–*C* and *SI Appendix*, Fig. S5). On the basis of those unique projections, we infer that the low-q reflection might be attributed to the formation of a new phase. As evidenced by simulated projections (Fig. 2 *A*–*C*, *Insets*), we speculate that a DP phase is formed. To further examine the suggested DP phase, three-dimensional imaging was acquired from the reconstruction of the TEM projections at which a characteristic hexapod texture for a DP phase can be clearly identified (Fig. 2*D* and *SI Appendix*, Fig. S7). Accordingly, the forming hexapod nodes evidence the existence of Schwarz primitive minimal surface and those unexpected projections were attributed to the projections viewing along [100], [111], and [321] directions. In contrast to the DD, the predicted reflections for the DP occur at the relative q values of $\sqrt{2}$:$\sqrt{4}$:$\sqrt{6}$: $\sqrt{8}$:$\sqrt{12}$: $\sqrt{14}$:$\sqrt{16}$: $\sqrt{20}$: $\sqrt{24}$:$\sqrt{38}$:$\sqrt{42}$ (marked by the black line) (Fig. 1*A*) at which the low-q reflection ($\sqrt{2}$ peak) is the (110) plane and an additional peak at $\sqrt{8}$ can be clearly identified as (220); note that there are the overlapping peaks from the DP with the DD such as$\sqrt{4}$:$\sqrt{6}$: $\sqrt{12}$ from the reflection planes of $(200)_{DP}$, $(211)_{DP}$, and $(222)_{DP}$. To unambiguously examine the suggested DP phase from the DD reflections without the concern of distortion or deformation, a two-dimensional SAXS pattern was acquired. As shown in Fig. 3, the Cartesian coordinates resolving from the reciprocal-space imaging reveal that there is no distortion on the cubic lattices for both DP and DD phases. On the basis of predicted scattering patterns with different zonal diffractions, the experimental results of the two-dimensional (2D) SAXS patterns clearly indicate that there are the [111] zonal diffraction, in particular with inner hexagonal spots in the low-q region attributed to the {110} of the DP phase, and the [110] zonal diffraction from the DD phase. Note that the diameter of the beam size for the synchrotron X-ray is ∼250 μm; as a result, the acquired diffraction is possible to give the coexistent reflections from the DP and DD phases. On the basis of 2D SAXS pattern, there is an obvious correlation on the [111] zonal diffraction of the DP phase and the [110] zonal diffraction for the DD phase with specific geometric relationship of the reciprocal lattices. To further clarify the coexistent DD and DP phases, three-dimensional reconstruction images were acquired by electron tomography in which the hexapod building unit for the DP phase while the tetrapod one for the DD phase can be also visualized as shown in Fig. 4. The epitaxial relationship (i.e., rhombohedral distortion from $[111]_{DP}$ to $[110]_{DD}$) thus suggests an order–order transition from the DP to DD phase in line with the experimental results from the solution casting with different evaporation rates.

Order–Order Transitions for Network Phases. To further investigate the thermodynamic stabilities of forming network phases, the solution-cast PS-*b*-PDMS with the coexistent DP and DD phases was examined under synchrotron radiation for temperature-resolved in situ SAXS experiments. As shown in Fig. 5, the characteristic reflection in the low-q region for the suggested DP phase and the corresponding reflections for the DP and DD phases can be clearly identified. Further increasing the temperature over 100 °C gives rise to order–order transitions. At the

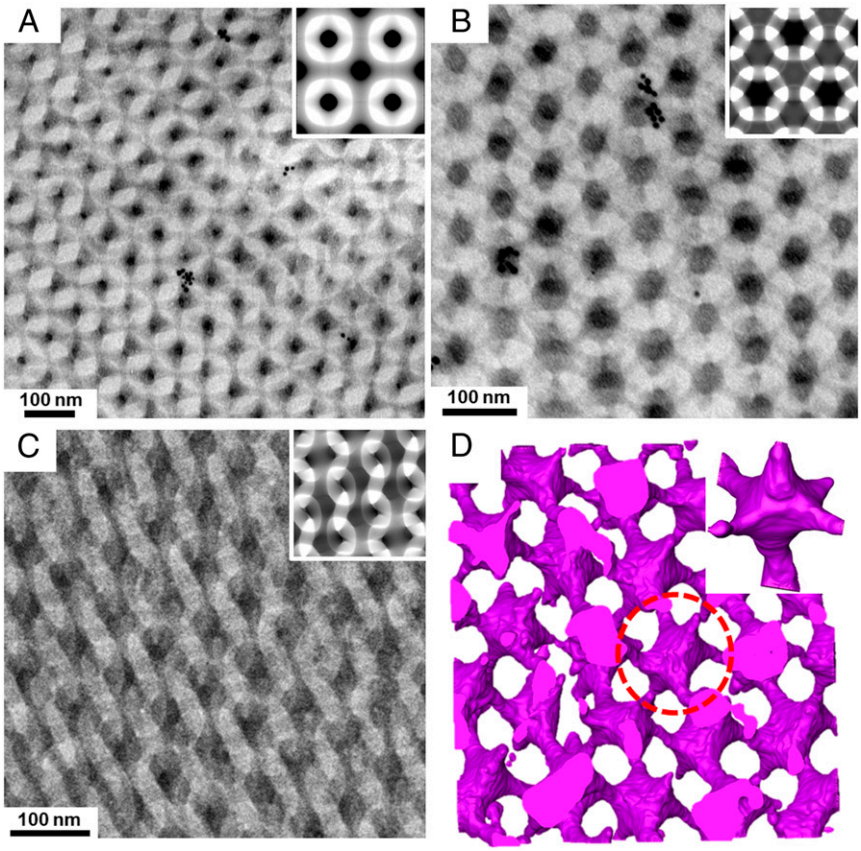

Fig. 2. TEM micrographs of fast-evaporated PS-*b*-PDMS along various projection directions: (*A*) [100]; (*B*) [111]; and (*C*) [321] for DP phase. (*Insets*) The corresponding images from simulation based on DP phase. (*D*) Three-dimensional reconstruction images of the kinetically arrested DP phase from PS-*b*-PDMS/SiO_2 along the [111] direction. (*Inset*) The building unit of the DP phase.

Downloaded by guest on February 15, 2022

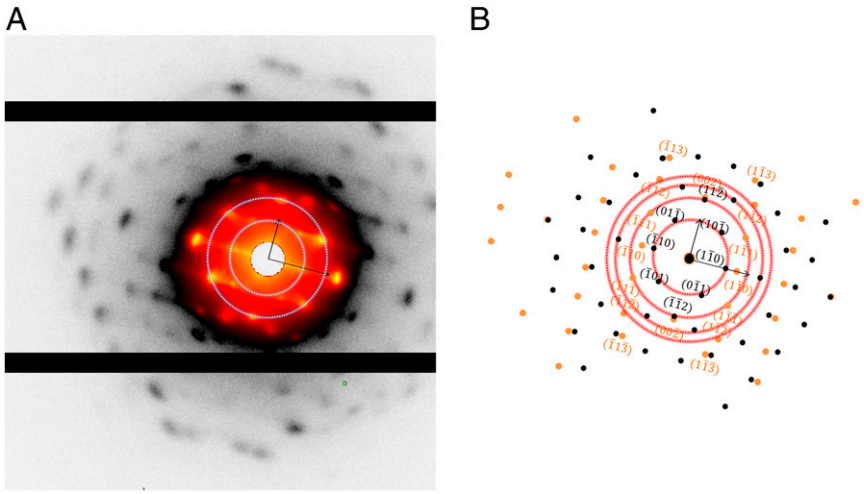

Fig. 3. (*A*) Two-dimensional SAXS pattern of the self-assembled PS-*b*-PDMS from fast evaporation; (*B*) the corresponding illustration of the coexistence of the [111] zonal diffraction of the DP phase (black dots) and the [110] zonal diffraction of the DD phase (orange dots).

beginning, an increase on the primary peaks of the DP phase [i.e., the reflection of $(110)_{DP}$] and that of the DD phase [i.e., the reflection of $(110)_{DD}$] can be found due to the devitrification of the PS matrix that gives rise to long-range ordering. A drop on intensity for the $(110)_{DP}$ can be recognized once the temperature reaches 130 °C, implicitly indicating the occurrence of transition from DP to DD phase (*SI Appendix*, Fig. S8 and see *SI Appendix* for details). As the temperature reaches 150 °C, the reflections from $(110)_{DP}$ and $(110)_{DD}$ start to be broadening and approaching toward each other simultaneously, suggesting the occurrence of order–order transitions from the coexistent DP and DD phases to a new phase. Once the temperature reaches 160 °C, the major characteristic reflections of the DP and DD phases would be extinct. After the temperature is over 160 °C, the completion of the phase transformation will give a significant reflection at low-q region, suggesting the formation of the DG phase [i.e., the reflection from $(211)_{DG}$ and $(220)_{DG}$]. The characteristic reflection planes for the DG were marked as the red dashed lines at the relative q values of $\sqrt{6}$:$\sqrt{8}$:$\sqrt{14}$:$\sqrt{18}$:$\sqrt{22}$:$\sqrt{32}$. To further examine the suggested DG formation, real-space imaging by TEM was carried out; as shown in Fig. 6 and *SI Appendix*, Fig. S11, characteristic [100], [110], [111], and [211] projections are evident. Moreover, on the basis of the reconstruction results, the transition zones from DP phase to DD phase (Fig. 4) and from DD to DG phase (*SI Appendix*, Fig. S10) could be clearly observed. Note that there is no evidence for the transformation from DP phase to DG phase (see below for detailed discussion).

Forming Mechanisms for DP Networks. On the basis of the microscopic examination, the DD phase takes the majority in the solution-cast bulk after fast evaporation. The trapped mixing phase with DD phase as a major one could be reasonably explained by considering that the DP phase with higher branch number (hexapod building unit) develops higher degree of packing frustration and therefore higher Gibbs free-energy state as compared to the one with tetrapod building unit (DD phase). According to the simulation results from self-consistent field theory (31), highly stretched polymer chains will be centered to the node and the interface will be adjusted to minimize the interfacial area resulting in packing frustration, which will be significant for the DP phase due to the larger volume of the hexapod. Consequently, the concentrating stress from extension of the PDMS block leads to the collapse of hexapods (31), giving a less-frustrated DD phase. Bonnet transformation has been extensively applied to elucidate the origins of phase transitions among the DD, DG, and DP phases (45), providing the rationale for the formation of the intermediate with rhombohedral distortion for illustration of the continuous transition path within the transition zone from DD to DP phase as observed under microscopy (35, 46, 47). In contrast to BCPs, owing to the lack of a crucial factor for consideration of the degree of stretching between two immiscible blocks to fill the space uniformly (entropic penalty), the phase transition path from Bonnet transformation contradicts the observed transition pathways in BCPs (48–50). Moreover, the hexapod nodes are indeed visibly larger than the tetrapod nodes and trigonal planar junctions as evidenced by the real-space image (Fig. 4), in line with the

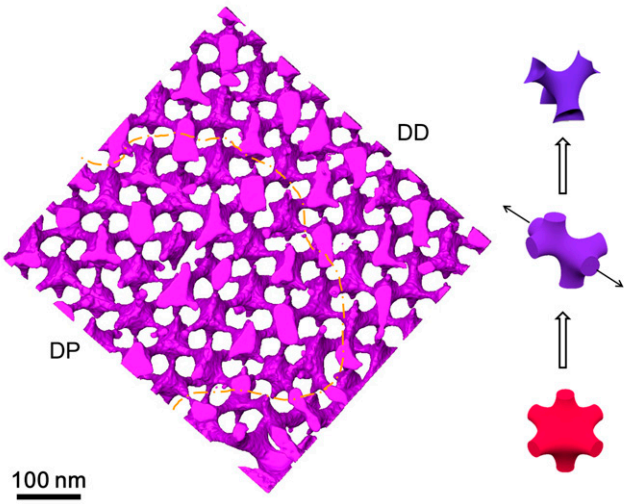

Fig. 4. Three-dimensional tomography of self-assembled PS-*b*-PDMS/SiO_2 from fast evaporation. The identified DP phase appears in the central area (projected along [111]) that is surrounded by the DD phase (projected along [110]). Rhombohedral distortion (as illustrated in purple) for continuous transition path within the transition zone from DP phase to DD phase with epitaxial relationship between $[111]_{DP}$ and $[110]_{DD}$ could be clearly identified. The boundary between the DP and DD phases is marked by the blue dashed line.

Downloaded by guest on February 15, 2022

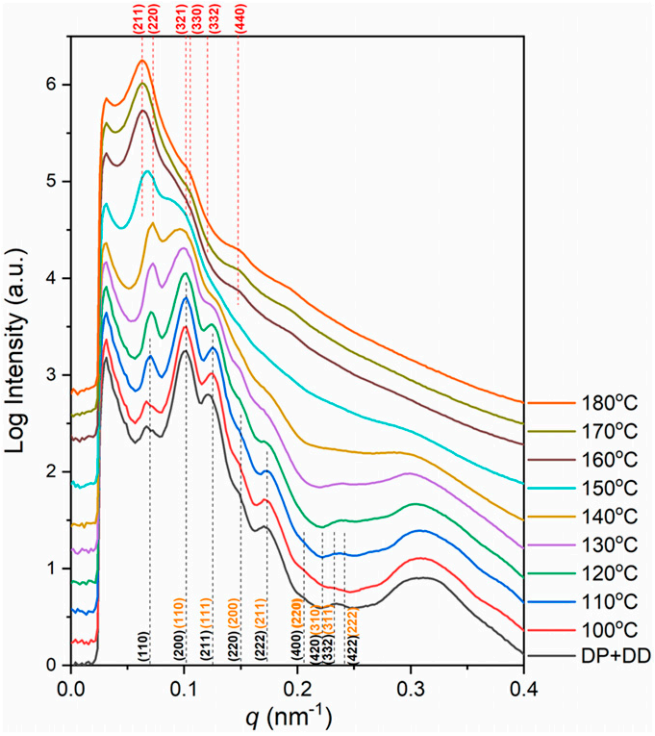

Fig. 5. Temperature-resolved in situ 1D SAXS profiles of PS-*b*-PDMS after fast casting. The red dashed lines are the reflection planes referred to $Ia\bar{3}d$ (DG). The orange brackets are the reflection planes referred to $Pn\bar{3}m$ (DD) at which an additional peak could be clearly identified in the low-*q* region. The black dashed lines are the reflection planes based on DP phase with $Im\bar{3}m$.

speculation that the higher the number of struts merging into the junction is, the larger the size of the junction (the node) will be (31, 38), at which the apparent deviation on curvatures from constant mean curvature suggests that polymer chains must be excessively stretched (51). Accordingly, we speculate that polymer with freely stretching chains (especially PDMS) might be kinetically trapped via the fast evaporation of a selective solvent (chloroform) (52), where the PDMS blocks might extend into the interior core of the junctions even with the loss of entropy from such high strut number network texture (i.e., DD and DP phase) (53, 54). As temperature rises, thermal energy attenuates χ value inducing fluctuations on the interfaces that relieve the concentrating stress, resulting in transformation into the DG phase.

Epitaxial Relationship among the DP, DD, and DG Phases. To further investigate the suggested order–order transitions, we purposely create the coexistent phases for the examination of the possible transformation mechanisms from fast evaporation of chloroform during the casting procedure, based on the inconsistency between simulated reciprocal-space imaging of the DD phase and the collected 2D SAXS pattern (Fig. 3). Furthermore, uniaxial distortion on the DD phase caused by shrinkage during the fast solution casting was excluded (43, 55). As a result, electron tomography could be conducted to acquire the real-space imaging as shown in Fig. 4. Explicitly, an epitaxial relationship [(i.e., rhombohedral distortion from $[111]_{DP}$ to $[110]_{DD}$)] can be clearly identified. The mechanisms for the order–order transition from a DP to DD phase based on simulations and experiments were thus justified. It is noted that for a Bonnet transformation from DD to DP, the epitaxial relationship will be given with the ratio of lattice constant for two morphologies (a^{DP}/a^{DD}) between 1.279 and 1.38 (35, 46, 47, 56). As determined from the $(200)_{DP}$ and $(110)_{DD}$ reflections, $a^{DP}/a^{DD} = \sqrt{2}\sim1.414$, reflecting that the phase transformation from a DP to DD phase might experience a "pulling-apart" process at which a hexapod node would be pulled along the [111] direction and then separated into two tetrapod nodes as demonstrated in Fig. 4. Similarly, it is intuitively believed that the order–order transition from a DD to DG phase undergoes the same pulling-apart process for transformation where a tetrapod node is pulled along the [100] direction into two trigonal planar network nodes. As shown in Fig. 5 and Table 1, the characteristic planes of DG shift toward low-*q* region, giving $d_{(211)}^{DG} = 100.37$ nm. The calculated a^{DD}/a^{DG} is ~2.81, far larger than that (a^{DD}/a^{DG} = 1.58 or 1.95) obtained from lipid systems showing minor effect from entropic penalty in general (47, 57). By contrast, in the case of the phase transition from DD to DG phase in semicrystalline BCPs (sPP-*b*-PS), the lattice constant ratio (a^{DD}/a^{DG}) is ~1.83 (29). We speculate that there will be no significant density variation upon phase transitions in the (PS-*b*-PDMS) system examined, as compared to the sPP-*b*-PS. As a result, it is reasonable to give a large ratio so that the large ratio may further evidence the suggested pulling-apart process for the transformation. Conclusively, the specific ratios of lattice constant for the pulling-apart transformation correspond to the suggested order–order transition sequence from a DP to DD phase, and finally to a DG phase at which no direct route for phase transformation from a DP to DG phase could be discovered.

Discussion

In conclusion, a series of cubic network phases can be obtained from the self-assembly of L-forming BCPs, PS-*b*-PDMS, after solution casting using a PS-selective solvent. Through faster evaporation of solvent, the DP phase could be kinetically trapped; in contrast, slow evaporation rate gives the formation of the DD phase. By taking advantage of thermal annealing, it is possible to experience peculiar order–order transitions from DP to DD phase and finally to DG phase. This discovery provides a perspective on the possibilities that highly packing frustrated morphology could be assembled from strongly segregated BCP

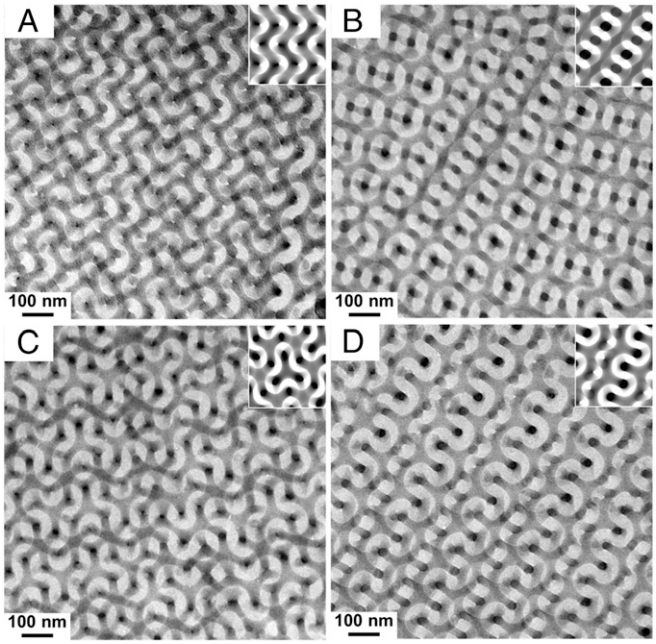

Fig. 6. TEM micrographs of solution-cast PS-*b*-PDMS after thermal annealing from various projection directions along (*A*) [100]; (*B*) [110]; (*C*) [111]; and (*D*) [211] for DG phase. (*Insets*) The corresponding images from simulation based on DG phase.

Downloaded by guest on February 15, 2022

Table 1. Summarization of *q* value of primary reflection plane, *d* spacing, the corresponding lattice constants of DP, DD, and DG phases, and the ratios of lattice constants

	DP	DD	DG
q value of the primary reflection plane, nm^{-1}	0.0704	0.1017	0.0626
Reflection plane	(110)	(110)	(211)
d spacing, nm	89.3	61.8	100.4
Lattice constant, nm	126.2	87.4	245.9
Ratio of lattice constants	$1.41(\sim\sqrt{2})$		2.81

systems, giving the feasibility to create network phases with controlled strut number.

Materials and Methods

Full synthetic methods and characterization details are provided in *SI Appendix*. The synthesis of the PS-*b*-PDMS diblock copolymer was accomplished by using anionic polymerization and high-vacuum techniques via sequential monomer addition. The synthesized PS precursor and PS-*b*-PDMS were characterized by size-exclusion chromatography, ^{1}H-NMR, and differential scanning calorimetry sequentially. Detailed information of characterization is combined in *SI Appendix*, Table S1. The following procedure for templated synthesis and the approaches to acquire reconstruction image from electron tomography are included in *SI Appendix*. Detailed analysis of the forming network structures by SAXS and electron tomography can be also found in *SI Appendix*.

Data Availability. All study data are included in the article and/or supporting information.

ACKNOWLEDGMENTS. We thank the Ministry of Science and Technology (MOST), Taiwan, for financially supporting this research under MOST 107-2923-M-007-003-MY3 and 107-2221-E-007-030-MY3 and the National Synchrotron Radiation Research Center for its assistance in the Synchrotron SAXS experiments. This work was supported in part by the Ministry of Education, Taiwan, ROC, under the Higher Education Sprout Project. The research work was supported by the Hellenic Foundation for Research and Innovation (HFRI) under HFRI PhD Fellowship Grant 1651.

1. F. S. Bates, Polymer-polymer phase behavior. *Science* **251**, 898–905 (1991).
2. F. S. Bates, G. H. Fredrickson, Block copolymers-designer soft materials. *Phys. Today* **52**, 32 (1999).
3. P. Vukusic, J. R. Sambles, Photonic structures in biology. *Nature* **424**, 852–855 (2003).
4. J. W. Galusha, L. R. Richey, J. S. Gardner, J. N. Cha, M. H. Bartl, Discovery of a diamond-based photonic crystal structure in beetle scales. *Phys. Rev. E Stat. Nonlin. Soft Matter Phys.* **77**, 050904 (2008).
5. J. W. Galusha, M. R. Jorgensen, M. H. Bartl, Diamond-structured titania photonic-bandgap crystals from biological templates. *Adv. Mater.* **22**, 107–110 (2010).
6. V. Saranathan *et al*., Structure, function, and self-assembly of single network gyroid ($I4_132$) photonic crystals in butterfly wing scales. *Proc. Natl. Acad. Sci. U.S.A.* **107**, 11676–11681 (2010).
7. H. Y. Hsueh *et al*., Shifting networks to achieve subgroup symmetry properties. *Adv. Mater.* **26**, 3225–3229 (2014).
8. K. Hur *et al*., Three-dimensionally isotropic negative refractive index materials from block copolymer self-assembled chiral gyroid networks. *Angew. Chem. Int. Ed. Engl.* **50**, 11985–11989 (2011).
9. S. Vignolini *et al*., A 3D optical metamaterial made by self-assembly. *Adv. Mater.* **24**, OP23–OP27 (2012).
10. Z. Gan, M. D. Turner, M. Gu, Biomimetic gyroid nanostructures exceeding their natural origins. *Sci. Adv.* **2**, e1600084 (2016).
11. L. J. Gibson, The mechanical behaviour of cancellous bone. *J. Biomech.* **18**, 317–328 (1985).
12. W. Huang *et al*., A natural impact-resistant bicontinuous composite nanoparticle coating. *Nat. Mater.* **19**, 1236–1243 (2020).
13. L. Wang, J. Lau, E. L. Thomas, M. C. Boyce, Co-continuous composite materials for stiffness, strength, and energy dissipation. *Adv. Mater.* **23**, 1524–1529 (2011).
14. J. H. Lee, L. Wang, M. C. Boyce, E. L. Thomas, Periodic bicontinuous composites for high specific energy absorption. *Nano Lett.* **12**, 4392–4396 (2012).
15. S. W. Robbins *et al*., Block copolymer self-assembly-directed synthesis of mesoporous gyroidal superconductors. *Sci. Adv.* **2**, e1501119 (2016).
16. M. Fruchart *et al*., Soft self-assembly of Weyl materials for light and sound. *Proc. Natl. Acad. Sci. U.S.A.* **115**, E3655–E3664 (2018).
17. E. L. Thomas *et al*., Ordered bicontinuous double-diamond structure of star block copolymers - a new equilibrium microdomain morphology. *Macromolecules* **19**, 2197–2202 (1986).
18. F. S. Bates, G. H. Fredrickson, Block copolymer thermodynamics: Theory and experiment. *Annu. Rev. Phys. Chem.* **41**, 525–557 (1990).
19. D. A. Hajduk *et al*., The gyroid: A new equilibrium morphology in weakly segregated diblock copolymers. *Macromolecules* **27**, 4063–4075 (1994).
20. T. H. Epps *et al*., Ordered network phases in linear poly(isoprene-b-styrene-b-ethylene oxide) triblock copolymers. *Macromolecules* **37**, 8325–8341 (2004).
21. T. H. Epps *et al*., Network phases in ABC triblock copolymers. *Macromolecules* **37**, 7085–7088 (2004).
22. T. S. Bailey, C. M. Hardy, T. H. Epps, F. S. Bates, A noncubic triply periodic network morphology in poly(isoprene-b-styrene-b-ethylene oxide) triblock copolymers. *Macromolecules* **35**, 7007–7017 (2002).
23. M. Takenaka *et al*., Orthorhombic Fddd network in diblock copolymer melts. *Macromolecules* **40**, 4399–4402 (2007).
24. X.-B. Wang, T.-Y. Lo, H.-Y. Hsueh, R.-M. Ho, Double and single network phases in polystyrene-block-poly(l-lactide) diblock copolymers. *Macromolecules* **46**, 2997–3004 (2013).
25. H. F. Wang *et al*., Networks with controlled chirality via self-assembly of chiral triblock terpolymers. *Sci. Adv.* **6**, eabc3644 (2020).
26. V. Z. Chan *et al*., Ordered bicontinuous nanoporous and nanorelief ceramic films from self assembling polymer precursors. *Science* **286**, 1716–1719 (1999).
27. R.-M. Ho *et al*., Block copolymers with a twist. *J. Am. Chem. Soc.* **131**, 18533–18542 (2009).
28. Y. Mogi *et al*., Preparation and morphology of triblock copolymers of the ABC type. *Macromolecules* **25**, 5408–5411 (1992).
29. C.-Y. Chu *et al*., Order–order transition between equilibrium ordered bicontinuous nanostructures of double diamond and double gyroid in stereoregular block copolymer. *Macromolecules* **45**, 2471–2477 (2012).
30. M. W. Matsen, F. S. Bates, Unifying weak- and strong-segregation block copolymer theories. *Macromolecules* **29**, 1091–1098 (1996).
31. M. W. Matsen, F. S. Bates, Origins of complex self-assembly in block copolymers. *Macromolecules* **29**, 7641–7644 (1996).
32. S. T. Hyde, Bicontinuous structures in lyotropic liquid crystals and crystalline hyperbolic surfaces. *Curr. Opin. Solid State Mater. Sci.* **1**, 653–662 (1996).
33. X. Zeng, G. Ungar, M. Impéror-Clerc, A triple-network tricontinuous cubic liquid crystal. *Nat. Mater.* **4**, 562–567 (2005).
34. A. Jain *et al*., Direct access to bicontinuous skeletal inorganic plumber's nightmare networks from block copolymers. *Angew. Chem. Int. Ed. Engl.* **44**, 1226–1229 (2005).
35. W. Mao, X. Cao, Q. Sheng, L. Han, S. Che, Silica scaffold with shifted "plumber's nightmare" networks and their interconversion into diamond networks. *Angew. Chem. Int. Ed. Engl.* **56**, 10670–10675 (2017).
36. P. D. Olmsted, S. T. Milner, Strong segregation theory of bicontinuous phases in block copolymers. *Macromolecules* **31**, 4011–4022 (1998).
37. E. W. Cochran, C. J. Garcia-Cervera, G. H. Fredrickson, Stability of the gyroid phase in diblock copolymers at strong segregation. *Macromolecules* **39**, 2449–2451 (2006).
38. F. J. Martínez-Veracoechea, F. A. Escobedo, Monte Carlo study of the stabilization of complex bicontinuous phases in diblock copolymer systems. *Macromolecules* **40**, 7354–7365 (2007).
39. M. Liu, W. Li, F. Qiu, A.-C. Shi, Theoretical study of phase behavior of frustrated ABC linear triblock copolymers. *Macromolecules* **45**, 9522–9530 (2012).
40. A. M. Urbas, M. Maldovan, P. DeRege, E. L. Thomas, Bicontinuous cubic block copolymer photonic crystals. *Adv. Mater.* **14**, 1850–1853 (2002).
41. C. Park, J. Yoon, E. L. Thomas, Enabling nanotechnology with self assembled block copolymer patterns. *Polymer (Guildf.)* **44**, 6725–6760 (2003).
42. T.-Y. Lo *et al*., Phase transitions of polystyrene-b-poly(dimethylsiloxane) in solvents of varying selectivity. *Macromolecules* **46**, 7513–7524 (2013).
43. X. Feng *et al*., Seeing mesoatomic distortions in soft-matter crystals of a double-gyroid block copolymer. *Nature* **575**, 175–179 (2019).
44. M. W. Bates *et al*., Stability of the A15 phase in diblock copolymer melts. *Proc. Natl. Acad. Sci. U.S.A.* **116**, 13194–13199 (2019).
45. A. Fogden, S. T. Hyde, Continuous transformations of cubic minimal surfaces. *Eur. Phys. J. B Cond. Matter Complex Syst.* **7**, 91–104 (1999).
46. J.-F. Sadoc, J. Charvolin, Infinite periodic minimal surfaces and their crystallography in the hyperbolic plane. *Acta Crystallogr. A* **45**, 10–20 (1989).

Downloaded by guest on February 15, 2022

47. A. M. Squires *et al*., Kinetics and mechanism of the interconversion of inverse bicontinuous cubic mesophases. *Phys. Rev. E Stat. Nonlin. Soft Matter Phys.* **72**, 011502 (2005).
48. S. Lidin, Symmetry restrictions on minimal-surfaces related by the bonnet-transformation. *Z. Kristallogr.* **188**, 121–129 (1989).
49. W. Mickel, G. E. Schröder-Turk, K. Mecke, Tensorial Minkowski functionals of triply periodic minimal surfaces. *Interface Focus* **2**, 623–633 (2012).
50. S. T. Hyde, S. Andersson, A cubic structure consisting of a lipid bilayer forming an infinite periodic minimum surface of the gyroid type in the glycerolmonooleat-water system. *Z. Kristallogr. Cryst. Mater.* **168**, 213 (1984).
51. D. M. Anderson, H. T. Davis, J. C. C. Nitsche, L. E. Scriven, *Periodic Surfaces of Prescribed Mean Curvature* (Springer, Berlin, 1987), pp. 130.
52. J. N. Lee, C. Park, G. M. Whitesides, Solvent compatibility of poly(dimethylsiloxane)-based microfluidic devices. *Anal. Chem.* **75**, 6544–6554 (2003).
53. W. Takagi *et al*., Bicontinuous double-diamond structures formed in ternary blends of AB diblock copolymers with block chains of different lengths. *Macromolecules* **52**, 6633–6640 (2019).
54. Y. Asai *et al*., Tricontinuous double diamond network structure from binary blends of ABC triblock terpolymers. *Macromolecules* **50**, 5402–5411 (2017).
55. G. E. S. Toombes *et al*., A re-evaluation of the morphology of a bicontinuous block copolymer–ceramic material. *Macromolecules* **40**, 8974–8982 (2007).
56. T. Oka, Transformation between inverse bicontinuous cubic phases of a lipid from diamond to primitive. *Langmuir* **31**, 3180–3185 (2015).
57. A. M. Seddon, J. Hallett, C. Beddoes, T. S. Plivelic, A. M. Squires, Experimental confirmation of transformation pathways between inverse double diamond and gyroid cubic phases. *Langmuir* **30**, 5705–5710 (2014).

Downloaded by guest on February 15, 2022